Predicting Millimeter Wave Radar Spectra for Autonomous Navigation

Ebi Jose, Martin Adams, *Senior Member, IEEE*, John Stephen Mullane, and Nicholas M. Patrikalakis, *Member, IEEE*

Abstract—**Millimeter Wave (MMW) radars are currently used as range measuring devices in applications such as automotive driving aids (Langer and Jochem, 1996), (Rohling and Mende, 1996), the mapping of mines (Brooker *et al.*, 2005) and autonomous field robotics (Brooker, 2001), (Langer, 1996). This recent interest is largely due to the advantages MMW radars offer over other range measuring sensors, as their performance is less affected by dust, fog, rain or snow and ambient lighting conditions. MMW radars can provide received signal strength values, at all discrete range intervals, within the working range of the radar (Clark and Durrant-Whyte, 1997), (Scheding *et al.*, 2002). The received power versus range spectra hence contain useful range to target information, but are also corrupted by noise. User defined stochastic algorithms can then be implemented, which exploit this rich data to improve object detection and mapping performance. This is in contrast to many other range measuring devices which typically internally threshold received signals, to provide single hard decisions only, on the estimated range to objects (Mullane, 2007).**

This paper addresses the issues of predicting the power-range spectra from MMW radars which use the Frequency Modulated Continuous Wave (FMCW) range estimation technique. This is important for two reasons. First, in automotive and autonomous robotic applications, such sensors are used in conjunction with vehicle navigation and map state estimation filters. This is so that (typically uncertain) vehicle motion knowledge can be optimally fused with the noisy sensor information, to infer estimates of the state of interest (typically, the vehicle's pose (position and orientation) and/or information of the surrounding object locations). Hence, it is essential that predicted power versus range spectra can be computed, to apply a Bayesian recursive estimation framework, based on previous measurements, and uncertain vehicle motion information. Second, it is extremely useful to be able to simulate MMW radar data, given certain environmental configurations. This aids the development of reliable object detection algorithms, based on theoretical sensor and noise models, which can then be applied more effectively to real MMW radar data.

Index Terms—**Millimeter wave RADAR, power range spectra, autonomous robotics.**

I. INTRODUCTION

COMPARED to other sensors commonly used for vehicle navigation such as laser range finders, vision systems or sonar, scanning Millimeter Wave (MMW) radar offers the advantage of higher reliability in bad weather or unpredictable lighting conditions. The radar used in this work is shown in Fig. 1, where it can be seen that the scanning swash plate and antenna are sealed inside a cylindrical perspex housing, which is almost opaque, making it insensitive to ambient lighting conditions. Evidence of a MMW radar's performance in heavy dust cloud (zero visibility) conditions, in a mining environment, is given in [9].

Some commercially available FMCW radars differ from other range sensors as they can provide complete power returns from an array of discrete range bins, for many points down range. In addition, MMW radar has a comparatively long range (hundreds of meters) which can enable a vehicle to navigate even with sparse features in its proximity. This paper provides the tools to predict MMW, frequency modulated, continuous wave (FMCW) radar, power-range spectra. This is achieved by theoretically analyzing the process of FMCW power versus range spectra generation including the effects of receiver noise on the range and power measurements.

For Bayesian autonomous navigation and map building, it is necessary to predict the target locations accurately given a prediction of the vehicle/radar location. A method for predicting such observations for an FMCW, MMW radar, based on estimates of the range to, and received power from, multiple line-of-sight targets is given in this paper. This is possible once prior robot and feature estimates are initialized, which include the vehicle's pose, the estimated feature locations and their radar cross section (RCS) estimates. Such predicted power versus range spectra will also prove extremely useful for simulating real data. The use of such simulated data can aid the quantification of feature detection algorithms, since random noise and clutter can be independently controlled. To achieve this, the simple radar range equation, modeling of the FMCW process and an experimental analysis of the power and range noise statistics are used.

This paper is organized as follows. In Section II, FMCW radar operation is explained, which provides an insight into the power versus range spectra generation and the noise they contain. This is essential for predicting the spectra correctly. Radar spectra prediction, using experimentally determined noise statistics during object absence is demonstrated in Section III. The aim is to generate realistic (with simulated noise) predicted radar spectra from predicted vehicle locations, with targets present. Section IV introduces an error metric, based on the Pearson Correlation Coefficient [10], for quantifying the accuracy of predicted power versus range spectra,

---

Manuscript received June 03, 2009; revised October 07, 2009; accepted November 09, 2009. Current version published March 26, 2010. The work was supported in part by the Singapore National Research Foundation (NRF) through the Singapore-MIT Alliance for Research and Technology (SMART) Center for Environmental Sensing and Modeling (CENSAM). The associate editor coordinating the review of this paper and approving it for publication was Prof. E. H. Yang.

E. Jose is with Singapore Technologies Electronics, Ltd., Singapore 569061 (e-mail: ebi@stee.stengg.com).

M. Adams and J. S. Mullane are with the School of Electrical and Electronic Engineering, Nanyang Technological University, Singapore 639798 (e-mail: eadams@ntu.edu.sg; jsmullane@ntu.edu.sg).

N. M. Patrikalakis is with the Department of Mechanical Engineering, Massachusetts Institute of Technology, Cambridge, MA 02139 USA (e-mail: nmp@mit.edu).

Color versions of one or more of the figures in this paper are available online at http://ieeexplore.ieee.org.

Digital Object Identifier 10.1109/JSEN.2009.2037013

Fig. 1. Photograph of the MMW radar used in the experiments. The antenna (located at the bottom of the unit) and swash plate (located in the cylindrical central section) are housed in an almost opaque perspex housing.

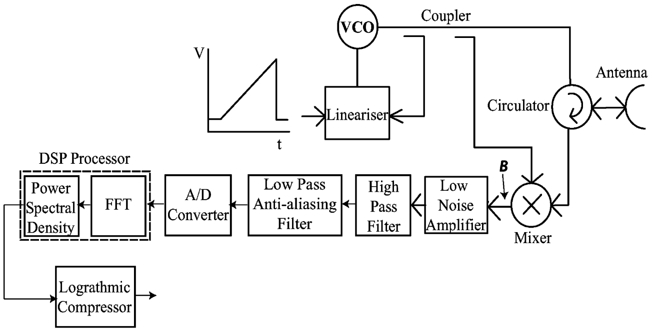

Fig. 2. Schematic block diagram of a MMW radar transceiver.

compared with actual data. The metric is used throughout the results in Section V. A comparison of the predicted and actual scans demonstrates the feasibility of the proposed radar spectra prediction techniques for providing spatial and received power predictions for trees, lamp posts, pillars, cars, and other artifacts in outdoor environments.

II. FMCW RADAR OPERATION

An introduction to the FMCW technique for obtaining target range is now given. This is necessary for radar signal interpretation and quantifying the noise in the range/power estimates. This is ultimately used in predicting range spectra observations given the predicted vehicle state, in a mobile robot navigation framework—which is the goal of this article. By analyzing the FMCW technique it will be shown which noise sources affect both the range and received power estimates, and how they are affected.

The transmitted power of the radar used here is 15 dBm and the swept bandwidth is 600 MHz [6]. Fig. 2 shows a schematic block diagram of an FMCW radar transceiver. In the figure, the input voltage to the Voltage Control Oscillator (VCO) is a ramp signal. The VCO generates a signal of linearly increasing frequency δf over a frequency sweep period T_d. This linearly increasing chirp is transmitted via the antenna. An FMCW radar measures the distance to an object by mixing the received signal with a portion of the transmitted signal [7]. The mixer output (point B in Fig. 2) then contains a signal, with beat frequency proportional to the target range. This signal is then passed through a high pass (range compensation) filter for ultimately obtaining a constant returned power value which is independent of range,[1] for a target of given RCS. Theoretically, assuming the simple radar equation (8) to be true, this would be achieved with a simple 40 dB/decade, high pass filter. This signal is then convolved with a Blackman window [11], to reduce the spectral leakage in the frequency spectrum output of the Fast Fourier Transform (FFT) processor [12]. Each element of the FFT result is multiplied by its complex conjugate to obtain the signal power spectral density. The logarithm of the power spectral density is then obtained to compress the large dynamic range of the power value estimates [5], which is the output of the radar.

A. FMCW Radar—Power Spectra Generation

The working principle of a standard FMCW radar receiver, which outputs received power-range spectra, is explained in this section. An in depth understanding of the spectra generation principle is essential for predicting the spectra.

Let the transmitted signal $v_T(t)$, as a function of time t, be represented as

$$\begin{aligned} v_T(t) &= [A_T + a_T(t)] \cos\left[\omega_c t + A_b \int_0^t t dt + \phi(t)\right] \\ &= [A_T + a_T(t)] \cos\left[\omega_c t + \frac{A_b}{2} t^2 + \phi(t)\right] \qquad (1) \end{aligned}$$

where A_T is the amplitude of the carrier signal, A_b is the amplitude of the modulating signal, ω_c is the carrier frequency (i.e., $2\pi \times 77$ GHz in this case), $a_T(t)$ is the amplitude noise and $\phi(t)$ is the phase noise present in the signal which occurs inside the transmitting electronic sections.

At any instant of time, the received echo signal, v_R is shifted in time from the transmitted signal by a round trip time, τ. The received signal is

$$\begin{aligned} v_R(t-\tau) &= [A_R + a_R(t-\tau)] \\ &\quad \times \cos\left[\omega_c (t-\tau) + \frac{A_b}{2}(t-\tau)^2 + \phi(t-\tau)\right] \qquad (2) \end{aligned}$$

where A_R is the received signal amplitude, $a_R(t-\tau)$ is the amplitude noise and $\phi(t-\tau)$ is the phase noise. The sources of noise affecting the signal's amplitude consist of external interference to the radar system (e.g., atmospheric noise, man-made signals) and internally produced noise at the receiver antenna and amplifiers.

In the mixer, the received signal is mixed with a portion of the transmitted signal in an analog multiplier, which can be mathematically described by

$$\begin{aligned} & v_T(t) v_R(t-\tau) \\ &\quad = [A_T + a_T(t)][A_R + a_R(t-\tau)] \\ &\quad \quad \times \left\{\cos\left[\omega_c t + \frac{A_b}{2} t^2 + \phi(t)\right]\right\} \\ &\quad \quad \times \left\{\cos\left[\omega_c (t-\tau) + \frac{A_b}{2}(t-\tau)^2 + \phi(t-\tau)\right]\right\}. \qquad (3) \end{aligned}$$

---

[1] Decreasing the dynamic range of the signal, necessary for further processing.

The output of the mixer, $v_{\text{out}}(t)$ is [2]

$$v_{\text{out}}(t-\tau) = \frac{[A_T + a_T(t)][A_R + a_R(t-\tau)]}{2} \times [B_1 + B_2] \quad (4)$$

where $B_1 = \cos[(2t-\tau)(\omega_c - (A_b\tau)/(2)) + A_b t^2 + \phi(t) + \phi(t-\tau)]$ and $B_2 = \cos[(\omega_c - A_b((\tau/2) - t))\tau + \phi(t) - \phi(t-\tau)]$.

The second cosine term, B_2 is the signal containing the beat frequency. The output of the low pass filter (which is intrinsic in the mixer stage) consists of this beat frequency component, B_2 and noise components with similar frequencies to the beat frequency, while other frequency components are removed. The beat frequency, f_{b_i} caused by the ith target down-range is directly proportional to the round trip time, τ. The relationship between the beat frequency and target range is

$$R_i = \frac{cT_s}{2}\frac{1}{f_s}f_{b_i} \quad (5)$$

where R_i is the range of the ith object, c is the velocity of the electromagnetic wave, T_s is the frequency sweep period, and f_s is the swept frequency bandwidth [13]. Hence, closer objects produce signals with lower beat frequencies and *vice versa*.

III. POWER-RANGE SPECTRA PREDICTION IN THE PRESENCE OF NOISE

Radar noise is the unwanted power that impedes the performance of the radar. For the accurate prediction of range spectra, the characterization of noise is important. It is, therefore, the aim of this section to introduce the type of noise distributions affecting the received chirp, and hence the received power and range estimates. The two main noise components are thermal and phase noise. Thermal noise affects the power reading while phase noise affects the range estimate.

Much of the robotics work which utilizes laser range finders, sonars or radars, naively adds uncertainty to the sensed range value only, which is typically assumed to be Gaussian. Based on a single range value, r_{meas}, and prior knowledge of the sensors range variance, ${\sigma_r}^2$, a likelihood of "target existence," Λ_{target} is formed as a function of range, r from the sensor, at each particular scanning bearing angle, given by

$$\Lambda_{\text{target}} = \frac{1}{\sqrt{2\pi}\sigma_r}\exp\left(-\frac{(r - r_{\text{meas}})^2}{2{\sigma_r}^2}\right). \quad (6)$$

This however does not take into account the uncertainty in detection, and therefore the true probability of existence of the detected target. If the probability density function is integrated over the range space, it would yield unity, meaning there is an inherent assumption that a target exists with complete certainty, somewhere within the range space. Even with sensors which output the received power value, as well as range (such as certain laser range finder models and radars), most of the robotics literature fails to make use of this value and assumes the above likelihood. Contrary to this school of thought, the noise in the MMW radar's received signal will be shown to have most affect on its *received power value* rather than its range estimate.

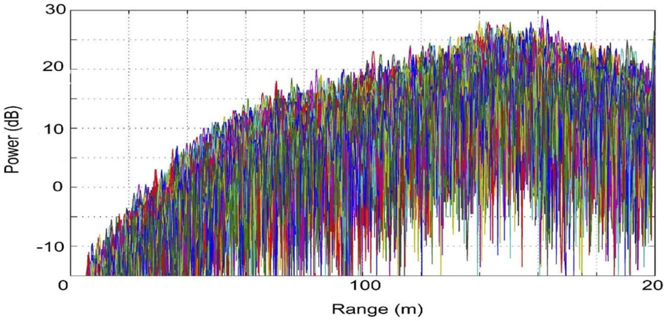

Fig. 3. Superimposed range spectra, for a constant radar swash plate bearing angle, with no targets present.

This is an important observation which translates to the fact that the received noise mainly affects the uncertainty in the very *existence* of an object being reported by the radar at a particular range, rather than the *range* value of the possible object itself.

The output of the filter within the mixer stage, which selects the difference frequency signal component within (4) is given by

$$v_{\text{beat}}(t,\tau) = \frac{A'}{2}\cos\left\{\left[\omega_c - A_b\left(\frac{\tau}{2} - t\right)\right]\tau + \Delta\phi(t,\tau)\right\} \quad (7)$$

where $A' = [A_T + a_T(t)][A_R + a_R(t-\tau)]$ is the product of the transmitted and received signal amplitudes, each corrupted with noise. $\Delta\phi(t,\tau) = \phi(t) - \phi(t-\tau)$ is called the differential phase noise which occurs due to the leakage of transmitted signals into the mixer [14].

Next, a brief discussion of the noise components present in the beat signal [shown in (7)] is given. This information is necessary in understanding the radar spectra and an effective representation of features.

A. Received Power Noise Estimation

As shown in (4), the beat frequency signal is affected by the thermal noise signal $a_R(t-\tau)$, which contributes to A' in (7) (point B in Fig. 2). Therefore this noise source directly corrupts the estimated received power.

Since the radar used is essentially a sealed black box, the method adopted to determine this noise (in terms of its distribution and parameter values) is to monitor several recorded power versus range spectra from the logarithmic compressor in Fig. 2 (the output of the radar). This is carried out by keeping the scanning swash plate stationary, and pointing into open sky (target absence). To determine the noise in the received signal, it is then necessary to reverse the effect of all of the signal processing blocks in Fig. 2 between the output and point B.

1) Received Power Noise Estimation During Target Absence: Fig. 3 shows 5000 actual superimposed range spectra output from the radar, obtained at a particular radar bearing angle, during target absence. The inverse operations of the final filtering stages in the receiver section of Fig. 2 were then applied to these spectra. This results in multiple time-domain signals, characterizing the noise present, before range compensation and logarithmic compression has taken place (i.e., at point B, after the

---

[2] Using the trigonometric identity for the product of two sine waves $\cos A\cos B = 0.5[\cos(A+B) + \cos(A-B)]$.

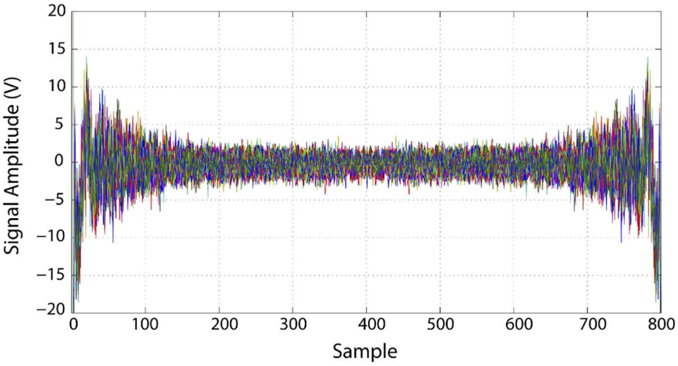

Fig. 4. Beat Signals in the time-domain (point B in Fig. 2) during target absence, obtained from the spectra with no targets present.

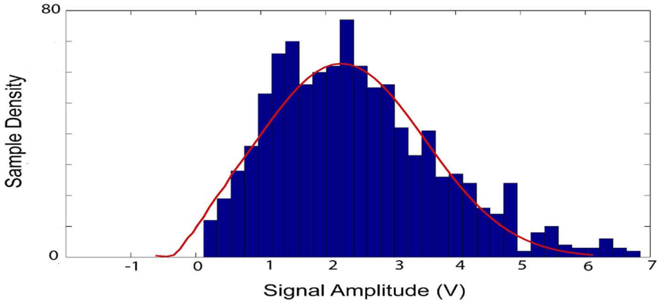

Fig. 5. Noise distribution at point B (in Fig. 2) during target absence, obtained from the spectra with no targets present. The distribution is approximately Rayleigh in nature and will be utilized in the spectra prediction method. Superimposed in red is the equivalent Rayleigh distribution with the same mean and variance as the discrete (blue) distribution.

mixer stage in Fig. 2). This involves removing the range compensation filter effect. It is then necessary to obtain the real part of the FFT from the power spectra, and apply the inverse Fourier transform to obtain the corresponding time-domain signal. Finally, removing the windowing effect (Blackman window) from the signals gives the time-domain signals at B. The resulting signals are shown in Fig. 4. These time-domain signals, are used to compute the noise statistics in the radar spectra. Due to the slight variation of the weights in the Blackman windowing process, the amplitude of the beat signals are higher at both the ends of the time-domain signal. The noise analysis is carried out in the central region of the graph of Fig. 4, where the windowing nonlinearities are minimal. The noise distribution then obtained at point B is as shown in Fig. 5. This distribution is approximately Rayleigh in nature[3] and the standard deviation of the Rayleigh noise is estimated as 1.25 V. As a first approximation it is reasonable to assume that the noise power statistics are independent of range and are dependent on the radar receiver electronics only, an approximation which has been verified experimentally [8]. The knowledge of the noise statistics during target absence (Fig. 5) is utilized in predicting the power spectra with multiple target returns, which is explained in the next section.

2) Predicting Noisy Power—Range Spectra With Targets Present: The power-range spectra, when target(s) are present can then be predicted by summing multiple, time-domain, sinusoids, with frequencies related to the range of each target given by (5). The mixer output then contains one or more beat frequencies f_{b_i} which correspond to the target range(s) R_i (given in (5)). The amplitude of each of these sine waves is proportional to P_{r_i}, which can be estimated by entering the predicted range R_i and RCS value σ_i into the simple radar equation (8)

$$P_{r_i} = \frac{P_t G^2 \lambda^2 \sigma_i}{(4\pi)^3 R_i^4 L} \tag{8}$$

where P_t is the radar's transmitted power, G is the antenna gain, λ is the wavelength, (i.e., 3.89 mm in this case) and L the radar system losses.[4] These predicted sinusoids, with frequencies f_{b_i} and amplitudes proportional to P_{r_i}, are then artificially corrupted with additive noise, generated according to the probability density function (PDF) of the received power range spectra during target absence. Finally, the filtering operations of the receiver, after point B in Fig. 2, are applied to the noise corrupted sinusoid(s) to give the final, noise corrupted, predicted power-range spectrum. This analysis makes the simplifying, but reasonable, assumption that the noise at point B in Fig. 2 primarily results from the components within the radar, and that it is independent of the environmental conditions (i.e., the same noise source (Fig. 5) is used to corrupt all power values).

B. Range Noise Estimation

Another source of noise which affects the range spectra is the phase noise $\Delta\phi(t,\tau)$ in (7). Phase noise is generated by the path leakage of the transmitted signal to the mixer, resulting in a spectrum of frequencies with finite bandwidth instead of a single beat frequency. This introduces noise into the range estimate itself, and experimental data shows that this results in a slight broadening of the power peaks along the range axis. This will be noticeable in many of the actual scans shown in Section V.

To demonstrate and estimate the phase noise effect, a large number (5000) of superimposed range spectra obtained for the same radar swash plate bearing angle are plotted together in Fig. 6. The top figure shows the entire range spectra with the returned power in dB,[5] while the lower figure shows the same set of range spectra using a linearly scaled power axis, with the effect of the range compensation filter removed. The Spectra contain three dominant features, observed due to the partial occlusion of objects, that lie inside the radar's beam width.[6] To estimate the phase (and hence range) noise distribution, a statistical analysis has been carried out on the targets (the peaks at approximately 10 and 136.5 meters), which also have differing RCS values, to determine any power and/or range dependency of the range noise statistics. The resulting range histograms are shown

---

[3] Two Gaussian noise sources, when passed through a mixer, result in Rayleigh noise [15], which explains the shape of the distribution in Fig. 5.

[4] The total system losses include atmospheric loss, beam-shape loss, beam-width factor, power fluctuation loss, miscellaneous signal processing loss and transmitter and receiver line noise [16]. The value of L is assumed to be 3 dB in this work.

[5] Note that the received power (dB) is a scaled value, which is proportional to the actual received to transmitted power gain.

[6] In Fig. 6 (top) (received power with a dB scale) three power returns are evident, due to the range compensation filter and logarithmic scaling. Clearly, after the power spectra is linearized and the range compensation filter effect removed, targets at higher range (such as the third target at 150 m) cannot be visualized on a linear scale, as shown in Fig. 6 (lower).

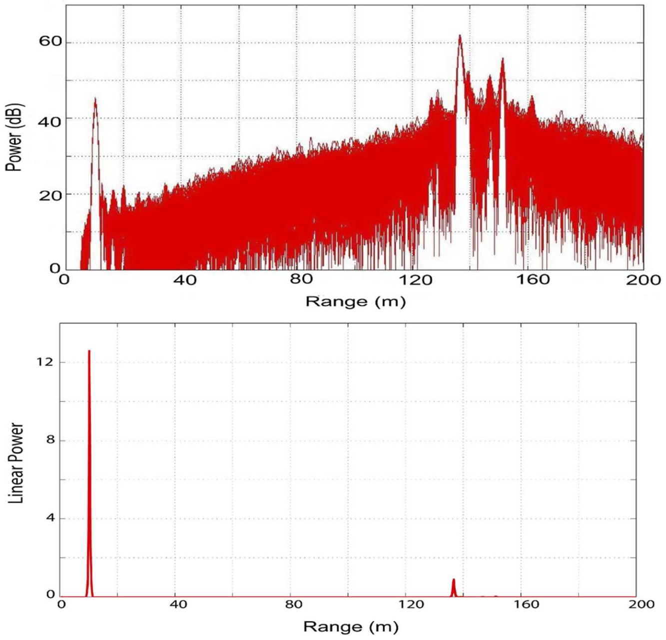

Fig. 6. 5000 range spectra plotted together for the same bearing angle. (a) Shows the power-range spectra in dB. (b) Shows the same power spectra with power values linearized, and the range compensation filter effect removed.

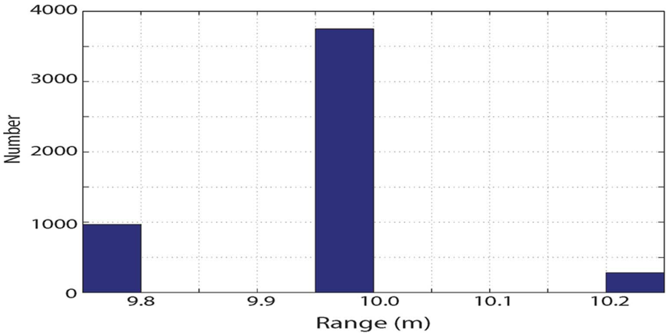

Fig. 7. Experimental histogram of range noise for an object at 10 meters.

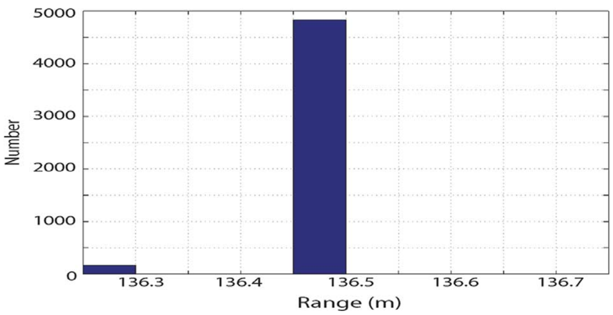

Fig. 8. Experimental histogram of range noise for an object at 136.5 meters.

in Figs. 7 and 8. The distributions show only the range values which correspond to the maximum power values recorded from a given target, with the radar swash plate fixed, taken from 5000 range spectra. It is apparent that the resulting range standard deviations are approximately independent of range and returned power, and more importantly, that they are significantly less than the range resolution (0.25 m) for this particular radar. Therefore, in the prediction of the radar range spectra, the broadening of peaks will not be considered significant in comparison with the range resolution of the radar's range bins, and the phase (and hence range) noise is ignored.

It is therefore reasonable to assume that the thermal noise which affects the received power value, plays a crucial role in the correct detection of a target. Feature/target extraction algorithms must be able to minimize the affect of this noise on target existence decisions.

The tools are now complete to predict radar spectra, given a robot navigation framework, capable of predicting the range to a target and its RCS.[7] This is possible given prior robot and feature estimates, which include the vehicle's pose, estimated feature locations and their RCS values. A Swerling I model is assumed, where the RCS values of objects are assumed to be omni-directionally constant with additive random fluctuations modeling RCS differences caused by the perspective from which the object is scanned [17]. In general this is clearly not a valid assumption, but becomes acceptable for small, cylindrical objects, making their RCS's approximately viewpoint invariant, such as lamp posts, trees, etc., which can be used for outdoor navigation.

IV. COMPARING PREDICTED AND ACTUAL SPECTRA

To quantify the "similarity" between a predicted power versus range spectrum, computed from previously recorded data from previous vehicle positions, and the current, corresponding real spectrum, the Pearson's coefficient of determination is used [10]. This coefficient provides a measure of the strength of the linear relationship between the predicted spectra X, with spectral values x_i, and the observed range spectra Y, with spectral values y_i, and will provide an indication of how accurate the predicted observations (spectra) are. This coefficient r_{xy}^2 $(0 < r_{xy}^2 < 1)$ is given by

$$r_{xy}^2 = \left[\frac{N\sum x_i y_i - \sum x_i \sum y_i}{\sqrt{\left(N\sum x_i^2 - (\sum x_i)^2\right)\left(N\sum y_i^2 - (\sum y_i)^2\right)}} \right]^2 \tag{9}$$

where each summation is taken from $i = 1$ to N with N being the number of bins in each power versus range spectra at a given scanning bearing angle (in this case $N = 800$). A value of $r_{xy}^2 = 1$ shows the two spectra are fully correlated and $r_{xy}^2 = 0$ shows that the two spectra are uncorrelated. Before determining this coefficient, the actual received spectrum under comparison is linearized, and then the effect of the range compensation filter removed, assuming it behaves as a 40 dB/decade, high pass filter, as mentioned in Section II. This allows comparison with a range uncompensated, linear power-range predicted spectrum. Due to the large dynamic range of the received signals however, for graphical comparison, the predicted and the actual spectra are still shown on a logarithmic scale, with range compensation applied (simulated with a 40 dB/decade, high pass filter on the predicted spectra).

---

[7] Which is theoretically proportional to the received power, assuming the range compensation, high pass filter to be ideal.

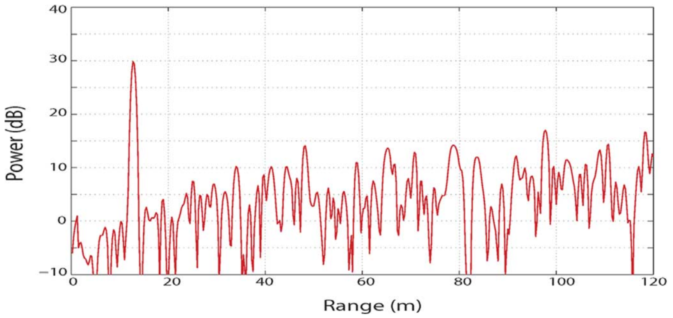

Fig. 9. Predicted Power versus range spectrum, for a single target, with a 40 dB/decade range compensation filter applied.

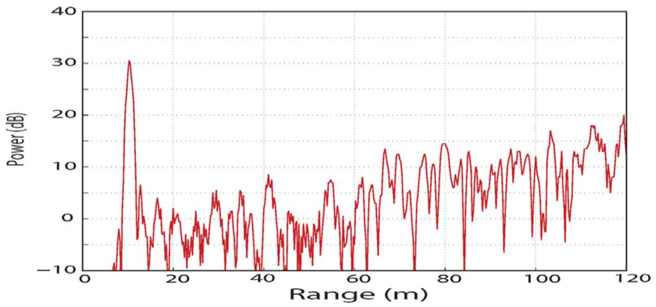

Fig. 10. Power versus range spectrum obtained from an actual target of RCS 10 m^2 at 10.25 meters.

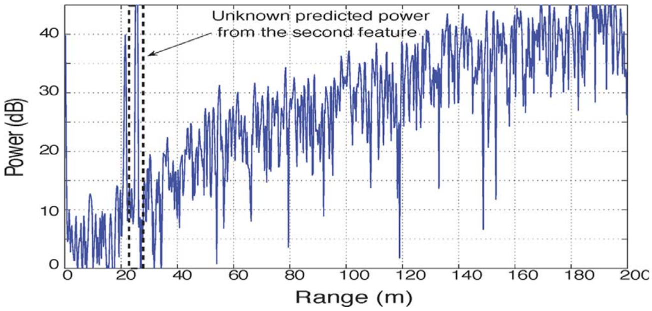

Fig. 11. Predicted power spectrum, for 2 co-aligned targets with a 40 dB/decade range compensation filter applied.

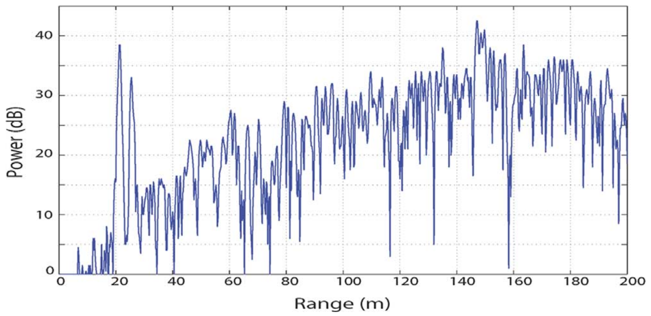

Fig. 12. Actual power spectrum obtained from the 2 co-aligned targets.

V. Results: Power-Range Spectra Prediction

A. Single Bearing Power-Range Spectra Prediction

1) Spectra Prediction From a Single Feature: As an example, a single power-range spectrum is to be predicted for an object with a known RCS (10 m^2), assumed to be at a distance of 10.25 meters from the radar. This will then be qualitatively and quantitatively compared with a real spectrum, recorded under the same conditions.

To generate the predicted observation, the beat signal corresponding to the object's range is artificially corrupted by Rayleigh noise, with the experimental parameters obtained from Fig. 5. The identical processing of the receiver elements after point B in Fig. 2, is then applied to this signal, to produce the returned power in dB shown in Fig. 9. Analysis of the predicted (Fig. 9) and actual range spectrum (Fig. 10) shows a slight mismatch in the noise frequency with respect to range. This mismatch is most likely due to the unmodeled phase noise throughout the entire range spectrum. It should also be noted that the actual radar used here is unable to report received power values for objects at ranges below 5 m, as can be seen in Fig. 10. The magnitude of the received power from the target (30 dB) corresponds to that actually received in the controlled experiment.

The r_{xy}^2 value [(9)] obtained for Figs. 9 and 10 is 0.9741, indicating a close similarity in the predicted and actual spectra.

2) Spectra Prediction From Multiple Features: If a predicted range spectra, contains multiple targets down-range, the predicted power from the first (closest) target only will be predicted correctly, since, in this work, no account is taken of the power absorption from the $N-1$ targets occluding the Nth target down-range. The prediction of the reduced power, which would be received from occluded targets has been addressed in [18].

Consider signal returns from multiple features[8]. The mixer output then contains multiple frequencies $(f_{b_1}, f_{b_2} \ldots, f_{b_N})$ which correspond to the ranges $(R_1, R_2 \ldots R_N)$ [given by (5)] to different objects. The power spectrum containing reflections from different objects can be predicted, as explained in Section V-A1. As an example, Fig. 11 (predicted spectrum) and Fig. 12 (real spectrum) show range compensated radar power spectra with reflections from two features. The first reflection is from a lamp post and the second reflection is from a tree.

For Figs. 11 and 12, $r_{xy}^2 = 0.9807$. This value indicates that the predicted range spectrum has a close "similarity" to the real spectrum with multiple features and that it is possible to predict power spectra with multiple feature returns accurately.

B. Full 360° Scan Spectra Prediction

This section compares the full 360° predicted radar scans with actual scans, obtained from outdoor terrains. The predicted full scans are then statistically compared with the actual ones to "*quantify the goodness*" of the proposed prediction method and the results are analyzed. Qualitative comparisons are also given, in terms of the known existence and position of objects within the scanned environments. The aim is to show how useful the predictive model is, based on detected features from an initial radar scan. These form an initial state which is then propagated through a vehicle kinematic model, together with the noise analysis, to produce predicted scans in other radar locations. The radar is then moved to that location, and a scan is taken for comparison purposes.

---

[8] Either due to the beam width or due to the radar wave penetrating closer objects.

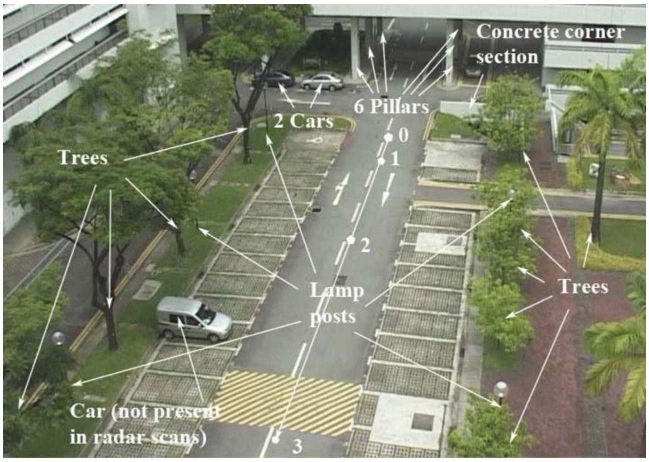

Fig. 13. Photograph of the car park environment used for comparing predicted and actual radar scans, with certain artifacts and natural objects labeled. Note that the car in the foreground was not present when the radar scans were recorded.

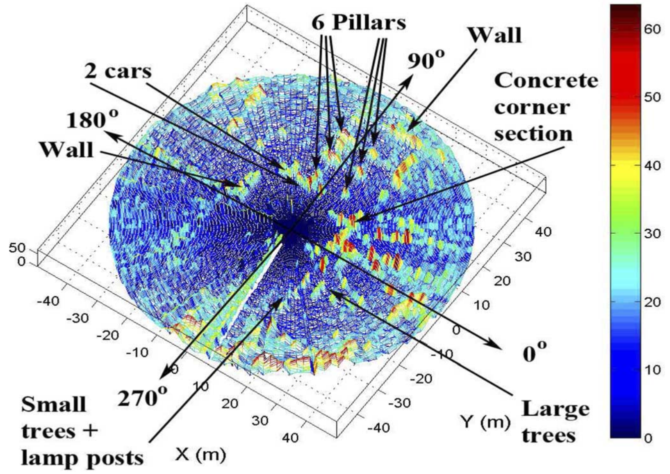

Fig. 14. 360° radar scan from the initial vehicle location "0" in Fig. 13, showing the power received from range values up to 50 m. The scale on the right indicates the received power values in dB. Features include trees, lamp posts, concrete buildings and pillars.

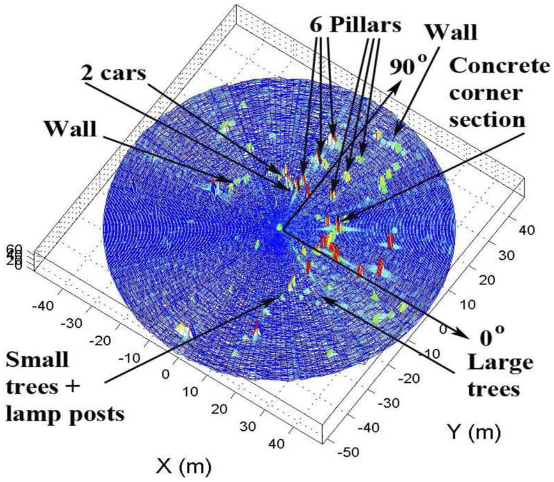

Fig. 15. Predicted 360° scan for the next predicted vehicle location, with predicted features labeled.

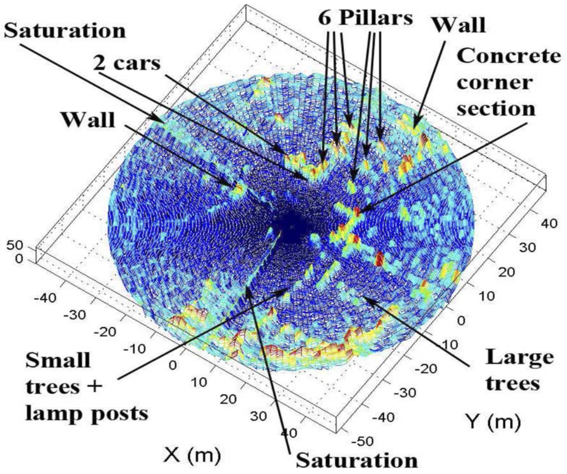

Fig. 16. Actual 360° radar scan from the outdoor environment, 2.3 m away (position "1" in Fig. 13) from the initial scan of Fig. 14.

For analyzing the proposed prediction method, tests have been carried out in an outdoor car park, shown in Fig. 13.

The real radar scan obtained from the initial vehicle location (marked "0" in the photograph) is shown in Fig. 14.[9] The color scale in the figure indicates the received power values. Features are extracted from this initial, raw scan using a cell averaging CFAR processor [19]. Next, the vehicle is moved and its location is predicted, based on odometry and the vehicle kinematic model [20]. A predicted scan is then calculated from that predicted vehicle location, by translating the previously extracted feature locations through the vehicle motion model, and using the above power-range spectra prediction method. The full predicted 360° scan from the car park is shown in Fig. 15. The vehicle is then commanded to move to that location (position "1" in Fig. 13) which is approximately 2.3 meters away from the initial location, and an actual radar scan is then obtained. This is shown in Fig. 16, in which certain identifiable objects are labeled for comparison with Fig. 15. From a qualitative point-of-view, it can be seen that artefacts such as the pillars, cars and concrete corner section correspond well between the predicted and actual scans. The most notable differences between them are caused by *spectrum saturation*, *phase noise*, and *clutter* present in the actual scan. Spectrum saturation occurs when a very high RCS target is present at a particular angle, which can cause the entire spectral power values, at that bearing, to be high, due to flooding of the receiver amplifier sections [3]. This is evident at the two labeled sections in Fig. 16. As mentioned in Section III-B, phase noise, which is also not modeled in our scan predictor, broadens the power peaks, thus increasing the uncertainty in the range at which objects are detected. This can be seen, as the received power from the wall, pillars, etc., are "widened" along their respective range axes of detection in comparison with their predicted values in Fig. 15. Clutter is also evident in the real data, and is not modeled in the predicted scans.

For quantifying the statistical similarity between the predicted and actual scans, again the correlation coefficient is obtained between each actual and predicted spectrum. The correlation coefficient r_{xy}^2 for the full scan is plotted at each bearing angle in Fig. 17, from which it is evident that relatively

---

[9] Note that the 360° scans, can be best visualized in color.

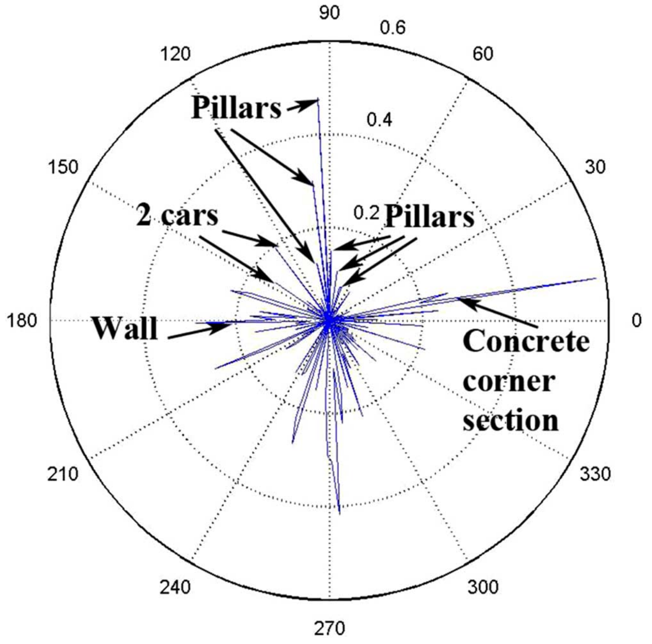

Fig. 17. Correlation coefficient of predicted and actual scans obtained from Figs. 15 and 16. Note that 0° corresponds to the 0° line marked in Fig. 15.

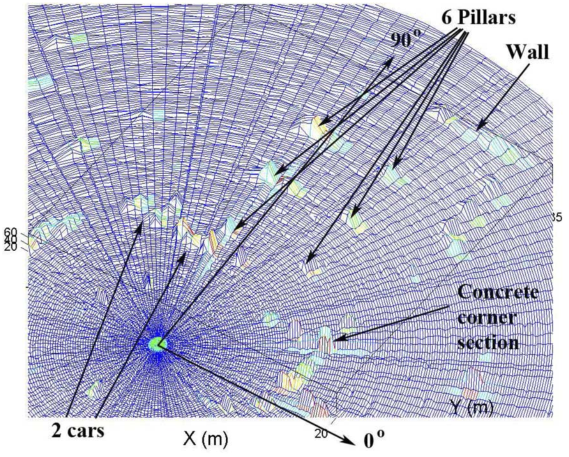

Fig. 18. A zoomed view of a section of the predicted scan of Fig. 15 showing the predicted power versus range spectra in the vicinity of the radar.

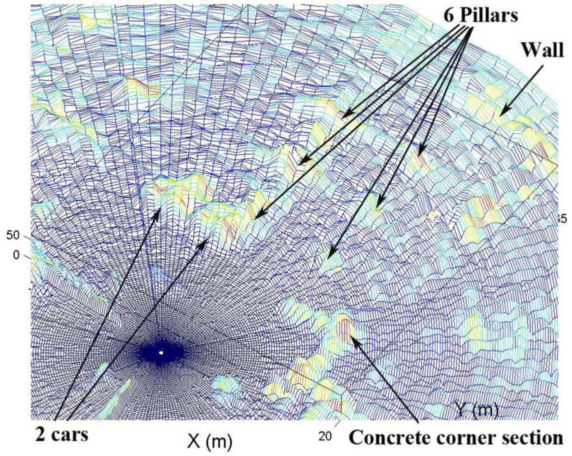

Fig. 19. A zoomed view of the corresponding section from the actual scan of Fig. 16.

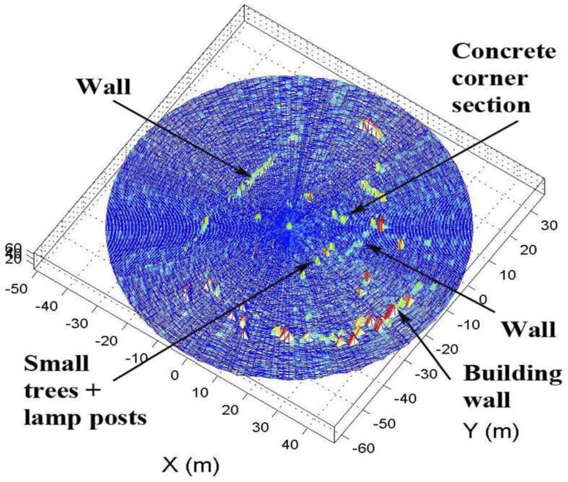

Fig. 20. Predicted radar scan from a vehicle location 11 meters away from the original scan of Fig. 14.

high (maxima) correlation values exist in the directions of the detected pillars, concrete corner section, large trees and a small section of the left wall. However, not all of the predicted spectra are correlated (or similar) with the real spectra, due to any of the following reasons:

- There is no clutter modeling incorporated into the prediction model. Hence, when a real spectrum, containing land clutter, is compared with the predicted one (with no clutter), a lower correlation results.
- Features may appear/disappear due to either partial occlusion of objects or due to object(s) being outside the radar's maximum visible range, at the position from which the predicted scan was computed.

Fig. 18 (which is a zoomed view showing the pillars, cars and concrete corner section labeled in Fig. 15) shows a more detailed view of these predicted artefacts. The corresponding zoomed actual scan is shown in Fig. 19. Again, in these scans, the main predicted and detected objects are clear as are the effects of phase noise and clutter in the real data. Importantly, robust objects are reliably predicted, making them suitable as features within robot navigation frameworks.

Fig. 20 shows the predicted 360° radar scan obtained from a vehicle location which is 11 meters away from the initial location. This is to show the usefulness of the predicted observations, for faster moving vehicles, or for slower prediction/update times, as it then becomes necessary to predict a scan at greater distances away from the data set used to compute it. The actual scan from that vehicle location is shown in Fig. 21. The correlation coefficient between each spectrum is shown in Fig. 22. As the vehicle moves from positions "1" to "2" in Fig. 13, the magnitude of the correlations in Fig. 22 in the directions of the concrete corner section, and the pillars are notably reduced, while those in the direction of vehicle motion, (corresponding to trees and lamp posts) increase. Again, importantly, most of the labeled features (which can be seen more clearly in the zoomed

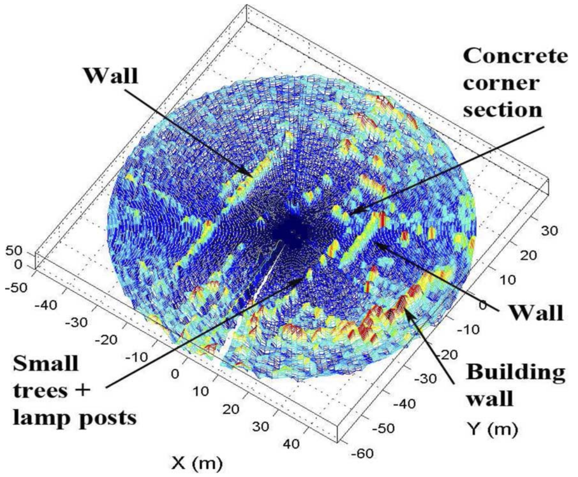

Fig. 21. Actual 360° radar scan after the vehicle drives 11 meters (to position "2" in Fig. 13) from the original location of Fig. 14.

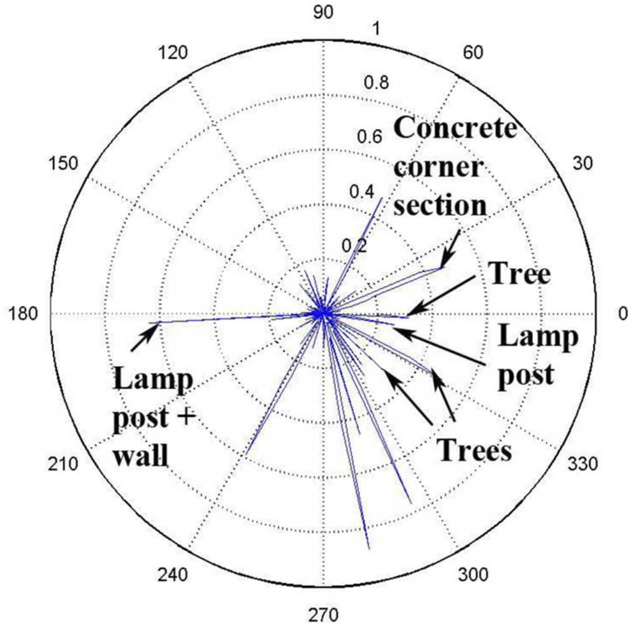

Fig. 22. Correlation coefficient of predicted and actual scans of Figs. 20 and 21.

views of Figs. 23 and 24) are accompanied by relatively high correlation coefficients (labeled in Fig. 22).

Finally, a predicted scan is generated for a large distance manoeuvre corresponding to 30 m of vehicle motion (placing the vehicle at position "3" in Fig. 13). As described in Section V-B, features extracted from the initial position ("0" in Fig. 13) are transformed using the vehicles odometry and the spectra prediction method to produce the predicted scan of Fig. 25. Note that a slight angular shift in the scan is apparent due to a slight vehicle rotation reported by the odometry.

When traversing such a large distance, one would expect less of the predicted features to match those in the real scan recorded at position "3" due to the occlusion or cluttering of distant objects recorded at position "0." Fig. 26 shows the actual scan recorded at position "3" along with the correlation coefficient plotted in Fig. 27, where it can be seen that robust features are still correctly predicted. The trees, lamp posts and a sign post, to the rear (between scanning angles 0° and 180°) of the vehicle at position "3," can be seen in both the predicted and actual scans,

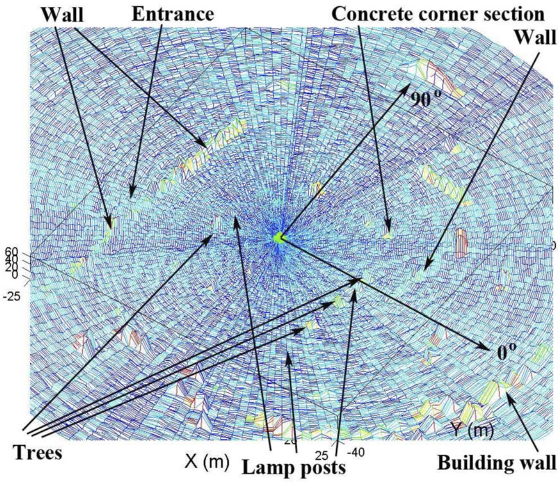

Fig. 23. A zoomed section of the predicted scan of Fig. 20 with labeled objects.

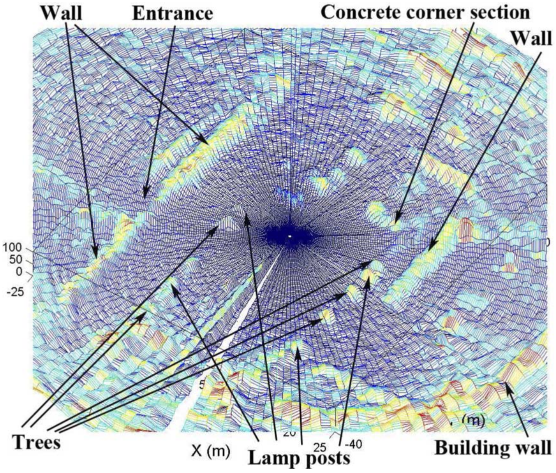

Fig. 24. A zoomed view of the corresponding section from the actual scan of Fig. 21.

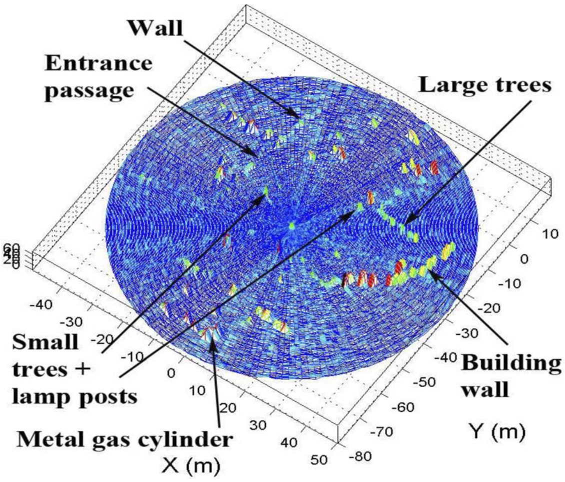

Fig. 25. Predicted radar scan 30 m from the position of the original scan of Fig. 14.

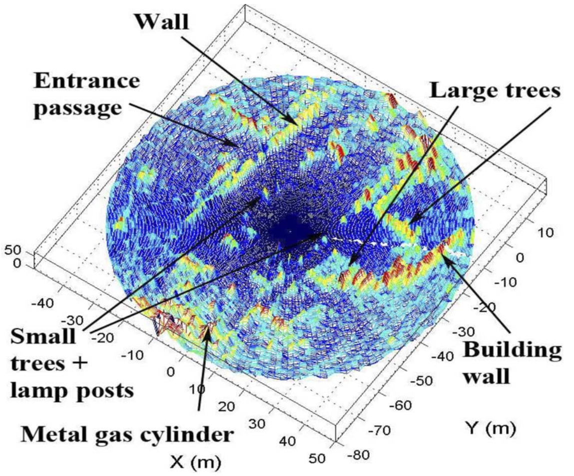

Fig. 26. Actual scan 30 m from the position of the original scan of Fig. 14.

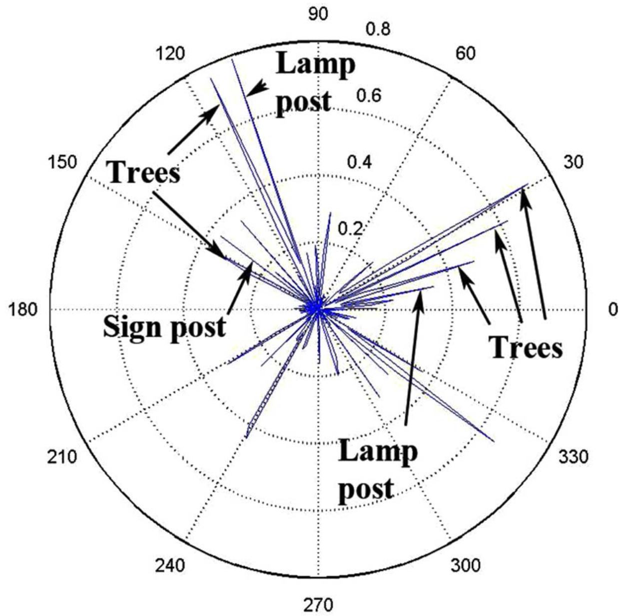

Fig. 27. Correlation coefficient of predicted and actual scans of Figs. 25 and 26.

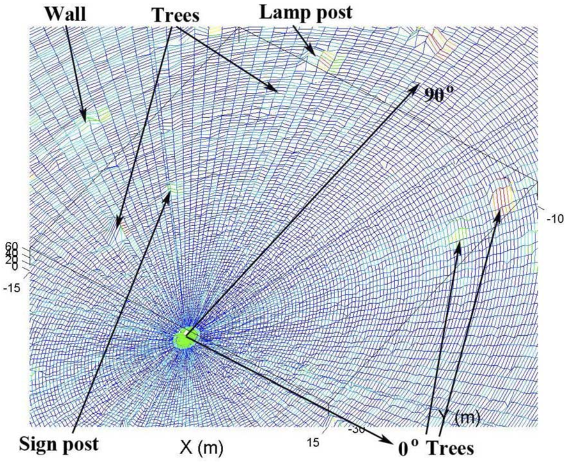

Fig. 28. A zoomed section of the predicted scan of Fig. 25 with labeled objects.

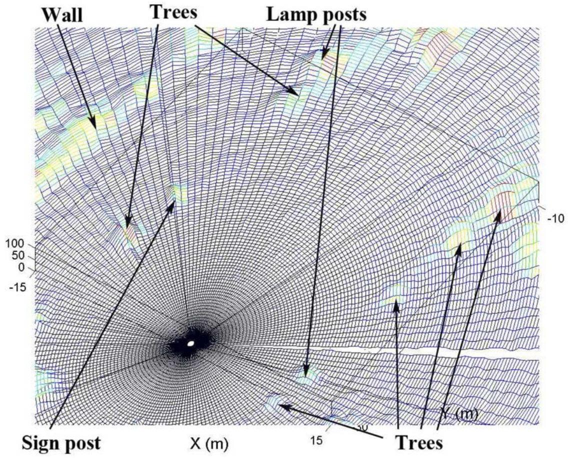

Fig. 29. A zoomed view of the corresponding section from the actual scan of Fig. 26.

and have correspondingly high correlation coefficients. This is logical, as this region is closer to the radar, when the scan was predicted at position "0." Figs. 28 and 29 show zoomed views in the vicinity of the robot with a clearer view of the successfully predicted trees, lamp posts and sign post, corresponding to the peaks in the correlation coefficient of Fig. 27.

It is observed in the correlation plots that the correlation coefficient of the same object is different in different scans. In reality, the RCS of most objects will change, as the sensor to object angle of incidence changes, which would also cause the correlation coefficient, for the same object, to change. It should also be noted that the correlation coefficient results from the correlation between an entire radar spectrum, at a given sensor bearing angle, which contains the object of interest, as well as noise and/or clutter. Hence, the predicted radar spectra, are created from the features sensed in one location, and propagated to another location, through the vehicle's kinematic model. These features will not, in general, lie in the same sensor bearing angles after the vehicle/sensor has moved, meaning that the new spectra containing the object of interest, are likely to contain radar data from other parts of the environment. If the new spectra contain clutter and/or other objects, the correlation coefficient will change. The important result here is that, at the locations of the predicted objects, the correlation coefficients contain maxima, indicating approximately correct feature predictions.

VI. CONCLUSION

A technique for predicting scanned MMW radar data, based on the FMCW range measurement technique, has been presented. This allows the development of an estimation framework in the raw, high dimensional, measurement space, as opposed to the reduced dimensional postprocessor, detection space. This is useful for two reasons.

1) Observations can be predicted for the purpose of data association, based on predicted vehicle manoeuvres. This is a fundamental component of stochastic autonomous navigation techniques, which requires the spatial prediction and then detection of targets, for vehicle pose and map estimation.

2) The methods can be adopted to simulate radar scans, in the presence of noise, for which different feature extraction algorithms can be tested, allowing the user to control target RCS values and the corrupting sensor noise parameters. Feature extraction algorithms (typically CFAR) require the noise within the neighboring bins of a feature to be estimated, which is why the prediction of entire spectra is useful. This also allows multiple line of sight features to be simulated.

Qualitative comparisons of predicted and actual scans were shown in the results, however, quantified comparisons provide more insight into the prediction quality. Therefore, a metric, based on the Pearson Correlation coefficient was utilized and demonstrated, which provided quantified comparisons, for validating the prediction technique. To test the concept, predictions of scans were made at progressively larger distances from the scan used to generate the predictions. Even at a distance of 30 m, robust feature prediction was demonstrated.

Further research, in which spectral saturation and clutter modeling would be useful for refining the model. This work is part of the authors' efforts in applying scanned MMW radar to probabilistic autonomous robot navigation in outdoor environments.

REFERENCES

[1] D. Langer and T. Jochem, "Fusing radar and vision for detecting, classifying and avoiding roadway obstacles," in *Proc. IEEE Symp. Intell. Vehicles*, Sep. 1996, pp. 333–338.

[2] H. Rohling and R. Mende, "Os cfar performance in a 77 ghz radar sensor for car application," in *Proc. CIE Int. Conf. Radar*, Oct. 1996, pp. 109–114.

[3] G. M. Brooker, S. Scheding, M. V. Bishop, and R. C. Hennessy, "Development and application of millimeter wave radar sensors for underground mining," *IEEE Sensors J.*, vol. 5, no. 6, pp. 1270–1280, Dec. 2005.

[4] G. Brooker, M. Bishop, and S. Scheding, "Millimetre waves for robotics," in *Proc. Australian Conf. Robot. Autom.*, Sidney, Australia, Nov. 2001, pp. 91–97.

[5] D. Langer, "An integrated mmw radar system for outdoor navigation," in *Proc. IEEE Int. Conf. Robot. Autom.*, Minneapolis, MN, Apr. 1996, pp. 417–422.

[6] S. Clark and H. F. Durrant-Whyte, "The design of a high performance mmw radar system for autonomous land vehicle navigation," in *Proc. Int. Conf. Field and Service Robotics*, A. Zelinsky, Ed., Sydney, NSW, Australia, 1997, pp. 292–299, Australian Robotic Association, Inc.

[7] S. Scheding, G. Brooker, M. Bishop, R. Hennessy, and A. Maclean, "Terrain imaging millimetre wave radar," in *Proc. Int. Conf. Control, Autom., Robot. Vision*, Singapore, Nov. 2002, pp. 13–18.

[8] J. Mullane, E. Jose, M. D. Adams, and W. S. Wijesoma, "Including probabilistic target detection attributes into map representations," *Robot. Autonomous Syst.*, vol. 55, no. 1, pp. 72–85, 2007.

[9] E. Widzyk-Capehart, G. M. Brooker, S. J. Scheding, R. C. Hennessy, A. J. Maclean, and C. R. Lobsey, "Application of millimeter wave radar sensor to environment mapping in surface mining," in *Proc. ICARCV*, Singapore, Dec. 2006, pp. 1–6.

[10] R. R. Wilcox, *Fundamentals of Modern Statistical Methods*. New York: Springer, 2001.

[11] A. V. Oppenheim and R. W. Schafer, *Digital Signal Processing*. Englewood Cliffs, NJ: Prentice-Hall, 1975.

[12] S. Clark, "Autonomous land vehicle navigation using millimetre wave radar," Ph.D. dissertation, Australian Centre for Field Robotics, Univ. Sydney, Sydney, Australia, 1999.

[13] D. Langer, "An integrated MMW radar system for outdoor navigation," Ph.D. dissertation, Robotics Institute, Carnegie Mellon University, Pittsburgh, PA, Jan. 1997.

[14] M. E. Adamski, K. S. Kulpa, M. Nalecz, and A. Wojtkiewicz, "Phase noise in two-dimensional spectrum of video signal in FMCW homodyne radar," in *Proc. 13th Int. Conf. Microw., Radar, Wireless Communi. (MIKON-2000)*, 2000, vol. 2, pp. 645–648.

[15] G. S. Bircsak and Schaaf, Van Nuys. Radar Clutter Simulator, Robotics Institute, Carnegie Mellon University, North Hollywood, CA, Tech. Rep. 4644357, Feb. 1987.

[16] M. I. Skolnik, *Radar Handbook*, 2nd ed. New York: McGraw-Hill, 1990.

[17] D. A. Shnidman, "Expanded swerling target models," *IEEE Trans. Aerosp. Electron. Syst.*, vol. 39, no. 3, pp. 1059–1069, Jul. 2003.

[18] E. Jose and M. D. Adams, "An augmented state slam formulation for multiple line-of-sight features with millimetre wave radar," in *Proc. Int. Conf. Intell. Robot. Syst.s (IROS)*, Alberta, Canada, Aug. 2005, pp. 1755–1760.

[19] V. G. Hansen and J. H. Sawyer, "Detectability loss due to greatest of selection in a cell-averaging CFAR," *IEEE Trans. AES*, vol. 16, pp. 115–118, 1980.

[20] M. W. M. G. Dissanayake, P. Newman, S. Clark, H. F. Durrant-Whyte, and M. Csorba, "A solution to the simultaneous localization and map building (slam) problem," *IEEE Trans. Robot. Autom.*, vol. 17, no. 3, pp. 229–241, Jun. 2001.

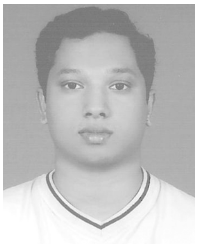

Ebi Jose received the B.S. degree in instrumentation engineering from the Cochin University of Science and Technology, Kerala, India, in 2002 and the Ph.D. degree from Nanyang Technological University, Singapore, in 2009. His thesis discusses the applications of millimeter wave radar for autonomous robot navigation.

Currently, he is a Senior R&D Engineer with S.T. Electronics (Satcom & Sensor Systems), Singapore.

Martin D. Adams (SM'08) received the B.A. degree in engineering science from the University of Oxford, Oxford, U.K, in 1988 and the D.Phil. degree from the Robotics Research Group, University of Oxford, in 1992.

He continued his research in autonomous robot navigation as a Project Leader and Part Time Lecturer at the Institute of Robotics, Swiss Federal Institute of Technology (ETH), Zurich, Switzerland. He was employed as a Guest Professor and taught control theory at St. Gallen (Switzerland) from 1994 to 1995. From 1996 to 2000, he served as a Senior Research Scientist in robotics and control, in the field of semiconductor assembly automation, at the European Semiconductor Equipment Centre (ESEC), Switzerland. He is currently an Associate Professor at the School of Electrical and Electronic Engineering, Nanyang Technological University (NTU), Singapore. He has published many articles in top ranking robotics journals and conferences, as well as various book chapters and a monograph. His research interests include sensor data processing for robot navigation, SLAM, inertial navigation and sensor fusion. He has been principle investigator of various robotics projects at NTU and acts as a consultant to various industries on autonomous robotic, intelligent transportation system and sensing applications.

John Stephen Mullane received the B.E. and Ph.D. degrees in electrical and electronic engineering from the University College Cork, Ireland, in 2002, and NTU, Singapore, 2009 respectively. His doctoral research focused on the development of robotic mapping and navigation algorithms using sensors prone to large uncertainty (both in measurement number and value) such as radar. His work specifically examined the theoretical foundation of measurement likelihoods adopted by existing approaches, he also proposed and demonstrated a random finite set approach for feature-based mobile robotics.

He is currently a Postdoctoral Research Fellow at the School of Electrical and Electronic Engineering, Nanyang Technological University (NTU), Singapore. His current research interests include radar signal processing, probabilistic mapping and stochastic mobile robotics.

Nicholas M. Patrikalakis (M'94) received the M.S. degree from the National Technical University of Athens, Athens, Greece, in, 1977 and the Ph.D. degree at the Massachusetts Institute of Technology (MIT), Cambridge, in 1983.

He is the Kawasaki Professor of Engineering and Professor of Mechanical and Ocean Engineering in the Department of Mechanical Engineering, MIT. His current research focuses on robotics and computer-aided design. Seventeen doctoral theses and 35 Master's theses have been completed under his direction. He has published over 140 papers, three textbooks, and has edited over 20 journal special issues or conference proceedings. He has received research funding from several federal agencies and industry in the USA and other countries. He serves as editor or member of the editorial board of four international scientific journals. He has also served as program chair or chair of over ten major international conferences and has participated in the program committees of over twenty international conferences.